Thermal characterization of modified uni-traveling carrier photodetectors: insights into temperature-dependent performance metrics

Ergun Simsek and Curtis R. Menyuk

Department of Computer Science and Electrical Engineering,
University of Maryland Baltimore County, Baltimore, MD, United States

ABSTRACT

We present an approximation method to compute the temperature distribution in photodetectors under steady-state optical excitation. The derived temperature profile assesses the impact on performance metrics like quantum efficiency, bandwidth, and phase noise. Our numerical study reveals that assuming constant room temperature leads to overestimated output current and quantum efficiency and underestimated bandwidth. In contrast, a varying temperature model closely aligns with experimental values. InGaAs's low thermal conductivity impedes heat dissipation, leading to temperature accumulation. Changing optical excitation while maintaining constant output current results in nonlinear changes in bandwidth, phase noise, and quantum efficiency. These findings aid in understanding and optimizing thermal management in photodetectors under strong optical excitations.

Keywords: photodetectors, photodiodes, heat

1. INTRODUCTION

Photodetectors (also known as photodiodes and abbreviated as PDs in the rest of this paper) are critical components in microwave photonics.[1–11] Achieving high radio frequency (RF) output power is challenged by saturation effects due to the space-charge effect[1,6] and heat-induced catastrophic failure.[10,11] Uni-traveling carrier (UTC) PDs have successfully addressed the space-charge effect, demonstrating enhanced high-power performance compared to traditional p-i-n PDs while maintaining high speed and linearity.[2] Modified uni-traveling carrier (MUTC) PDs, with a distinctive cliff layer controlling the electric field strength in absorber and collector regions, have further improved space-charge tolerance.[3–5] Researchers also found that the responsivity of both UTC and MUTC PDs increased due to an increased photoabsorption coefficient at elevated operating temperatures.[3] However, temperature-dependent bandwidths varied depending on the thicknesses of the p and i layers due to competing effects such as reduced carrier saturation velocity in the undoped or lightly-doped photoabsorption layer and increased electron diffusion in the p-type layer at higher temperatures.[3]

Despite these advances, higher RF output power is still limited by thermal challenges. This paper examines the thermal characteristics of conventional backside-illuminated MUTC PDs, focusing on the MUTC2 variant.[5] This PD has achieved notable results, including a quantum efficiency of 0.55 and a bandwidth of 24 GHz.[5] In another study,[4] researchers used a thermal-reflectance imaging system to characterize the surface temperature of the MUTC2 and implemented a simulation model using a commercially available finite element analysis tool, obtaining numerical results in good agreement with measured temperature distributions. Another study examined a variant of MUTC PD at three temperature regimes (300 K, 80 K, and 4 K) and multiple bias conditions,[8] finding that both responsivity and bandwidth decrease with decreasing temperature. Numerous publications present experimental[12–17] and numerical[18–21] results on the characterization of other PD types (such as $p-i-n$ and Avalanche PDs) as a function of temperature. Numerical models fall into two categories: one assumes a constant temperature for the entire PD,[19,20] which may suffice for simple PDs like p-i-n but is inadequate for multi-layered PDs. The other includes temperature as a variable, affecting material properties, carrier concentrations, fields, and currents.[12–14,18] This latter approach is thorough but complex. We aim

Further author information: (Send correspondence to E. S.)
E-mail: simsek@umbc.edu, Telephone: 1 410 455 3540

for a more simplified approach to estimate the temperature distribution within PDs and provide insights into temperature-dependent performance.

In the following sections, we briefly present our methodology, numerical results, and implications for improving high-power PDs in future photonic microwave applications. We also explore temperature-dependent changes in quantum efficiency, RF output power, and bandwidth, as revealed by previous experimental studies. Our numerical model allows us to investigate the impact of temperature on the performance metrics of MUTC2 PD, enhancing our understanding of the thermal challenges associated with these advanced devices.

2. NUMERICAL MODEL

We solve drift-diffusion equations to study PDs,[22,23] starting with the electron and hole continuity equations and the Poisson equation. The details on the formulation[22] and broadband radio frequency (RF) output calculations in a single simulation[23] were reported previously. Here, we describe a simple addition to our drift-diffusion equations solver to estimate the temperature distribution over a photodetector, focusing on the MUTC2 design.[4,5] This PD comprises InP, InGaAs, and InGaAsP layers with varying thickness and doping concentrations.[5,24]

The heat transport equation describing the spatiotemporal dynamics of the temperature distribution in the photodetector is:

$$c_H \frac{\partial T}{\partial t} - \nabla \cdot \sigma_T \nabla T = H \tag{1}$$

where T is the temperature, c_H is the volumetric heat capacity, σ_T is the thermal conductivity, and H is the heat generation rate. The c_H and σ_T values or formulas for InP, InGaAs, and InGaAsP are provided in Table 1.

Table 1. Heat capacitance and thermal conductivity of semiconducting materials that are used in the MUTC2 design.

Material	c_H **(J/gK)**	σ_T **(W/cmK)**
InGaAs	0.3	See Eq. (2)
$Ga_{0.47}In_{0.53}As_yP_{1-y}$	$0.31 + 0.038y - 0.008y^2$	$0.68 - 1.77y + 1.25y^2$
InP	$0.28 + 10^{-4}T$	$0.68(300/T)^{1.4}$

We use a temperature-dependent thermal conductivity model for InGaAs given by the following equation

$$\sigma_T(T) = \sum_{i=1}^{3} a_i \exp\left[-\frac{(T-b_i)^2}{c_i^2}\right], \tag{2}$$

since the absorption occurs in the InGaAs layers, where the electric field is expected to be strong. The coefficients of this equation, listed in Table 2, are extracted from experimentally measured results.[25]

Table 2. The coefficients used in Eq. (2) to calculate the thermal conductivity of InGaAs as a function temperature, T.

i	a_i	b_i	c_i
1	0.6204	194.1	86.21
2	1.159	197	180.9
3	4.959	-9.86	1044

The bandgaps of the semiconductors, the number of electrons and holes in the conduction and valence bands, and low-field mobilities and saturated velocities of the holes and electrons are also calculated as functions of temperature.[24]

We note that Eq. (1) requires boundary conditions. Also, one must consider interfaces and numerous complex mechanisms for a time-dependent study. However, for an approximate temperature distribution in a steady-state photodetector, Eq. (1) simplifies to:

$$-\nabla \cdot \sigma_T \nabla T = \mathbf{J} \cdot \mathbf{E} \tag{3}$$

where $\mathbf{J}$ is the local electric current. Using thin layers with thickness δz to describe a semiconductor device (where $\delta z \ll \lambda$), this simplified expression indicates that the local temperature change in the i^{th} thin layer is approximated as:

$$\nabla T_i \approx -\frac{\delta z}{\sigma_T}(\mathbf{J} \cdot \mathbf{E}). \tag{4}$$

Assuming a constant temperature at the p-contact (because the photodetector is illuminated from the n-side), we impose a Dirichlet boundary condition at $z = 0$. Using Eq. (4) to approximate the temperature derivative imposes a Neumann boundary condition at each interface of the one-dimensional (1D) mesh.

In our iterative approach, we use Eq. (4) for each layer of our 1D mesh and update the local temperature in each iteration. The material properties, such as thermal conductivity, heat capacity, electron and hole diffusion coefficients, mobilities, velocities, band gap, and electrical permittivity, are recalculated using the updated local temperature for each layer.

3. NUMERICAL RESULTS

For the numerical results presented here, we assumed a load resistance of 50 Ω. The PD has a diameter of 34 μm and is excited from the top (from the n-side) with an optical excitation wavelength of 1550 nm. The beamwidth of the excitation matches the PD diameter. A non-uniform mesh[22] with a maximum grid spacing of 1 nm was used for both steady-state and RF output power calculations. For broadband calculations, the time step size was set to 0.1 ps.[23]

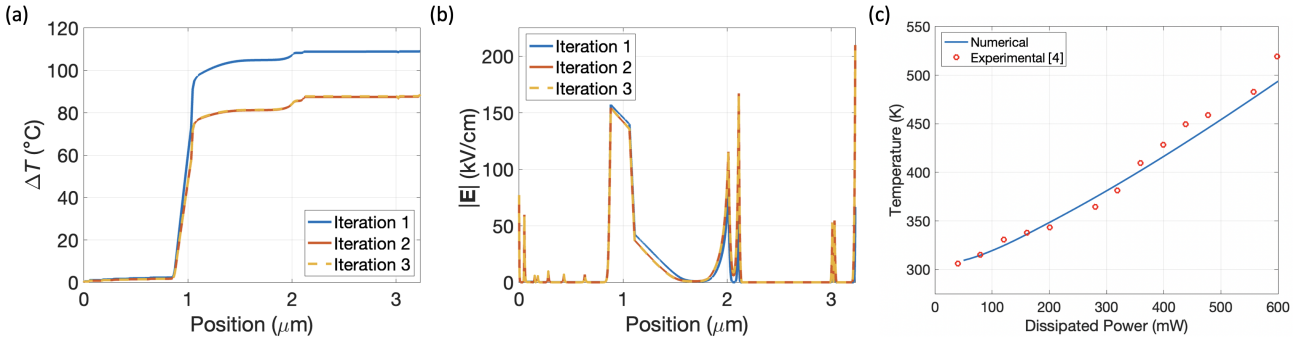

Figure 1. (a) Temperature distribution over the photodetector at the end of the first three iterations. (b) Electric field distributions over the photodetector at the end of the first three iterations. (c) Temperature of the n-contact as a function of dissipated power. Experimental and simulation results are taken from.[4]

To evaluate the precision of our method, we performed a numerical study of the MUTC2. Initially, we assumed a constant temperature of 300 K throughout the device and computed the local electric fields and currents at a −5 V reverse bias. Subsequently, we determined the local temperature variations in each cell of the mesh using Eq. (4). Given that the device is illuminated from its n-side, we summed these ∇T_i values cumulatively to acquire the overall temperature change (ΔT) from the p-side to the n-side, as illustrated by the blue curve in Fig. 1 (a). We then reran our drift-diffusion equations solver, this time using the local temperature as $T + \Delta T$. The red curve in Fig. 1 (a) shows a lower temperature distribution in the PD than in the initial iteration. Repeating this process five more times, we observed the temperature profile stabilized after the third iteration, i.e., $\Delta T < 0.001$°C. Figure 1 (b) presents the calculated electric field distributions for each iteration. As anticipated, the electric field intensity is substantial within the absorber (InGaAs) layers, where we also notice a significant shift in the temperature profile. The primary cause for this abrupt temperature change (Fig. 1 (a)) is the very low thermal conductivity of InGaAs. This low thermal conductivity hampers heat flow, leading to temperature accumulation. Additionally, Fig. 1 (b) shows abrupt changes in electric field intensity, which occur when the material type changes and/or the doping concentration shifts dramatically.[1–3,5,7,22,23,26] For the final stage of our initial study, we calculated the temperature, field, and current distributions over the photodetector, assuming a wide range of optical excitations. We maintained the p-contact of the photodetector at 15°C. The temperature at the n-contact as a function of dissipated power, calculated by our model, is shown by the blue

curve in Fig. 1 (c). The red circles represent the experimental measurements.[4] There is a notable agreement between the numerical and experimental results, but the disparity between numerical and experimental findings becomes more significant as power increases. Beyond our model's inherent approximations, several other factors could contribute to this deviation. For instance, the simplified geometry may not fully capture the complexities of the actual device structure, or the boundary conditions for heat transfer may vary. At higher power levels, the convective heat transfer rate, which we have not included, might increase nonlinearly due to larger temperature differentials. A three-dimensional dynamic model that incorporates both conduction and convection currents is needed to enhance accuracy.

Although we did not integrate our dynamic drift-diffusion equations solver[22,23] with a heat-transport model, we explored how the results would differ by assuming a constant temperature distribution versus a temperature distribution that varies according to Eq. (4).

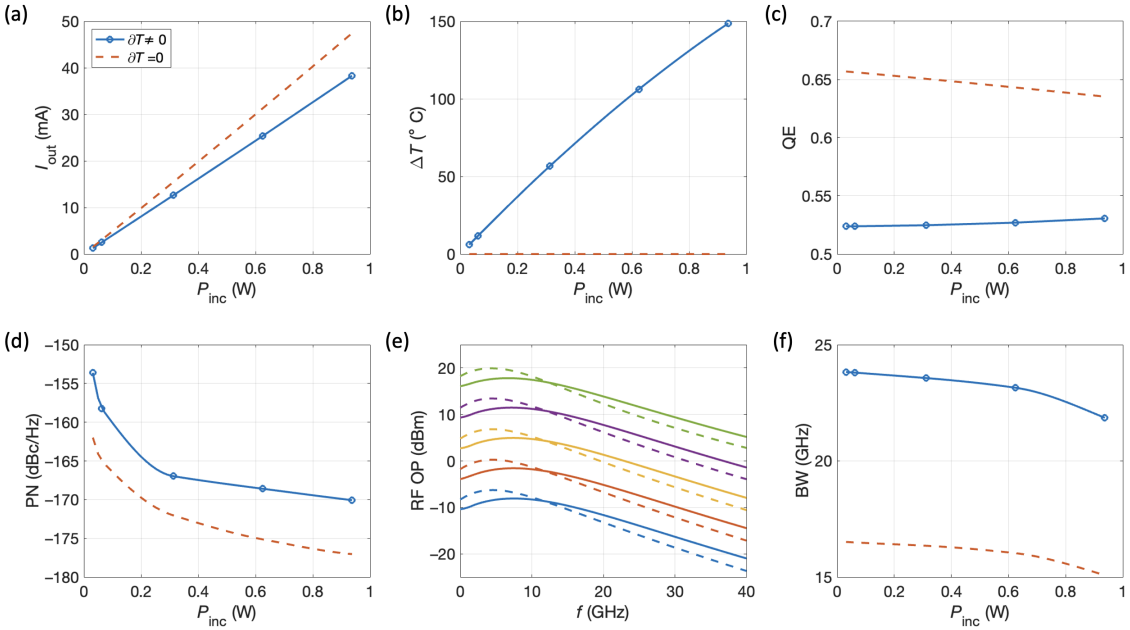

Figure 2. (a) Output current, (b) temperature change at the n-contact, (c) quantum efficiency, (d) phase noise, (e) RF output power, and (f) bandwidth of the MUTC2 calculated by assuming a constant temperature (dashed curves) vs. varying temperature (solid curves).

We first set the bias voltage (V_b) to 4 V and ran our code at five incident power levels (31 mW, 62 mW, 310 mW, 620 mW, and 930 mW) twice. In the first set, we assumed a constant temperature, $T = 300$ K. In the second set, we used Eq. (4). As we increased the intensity of the incident light, more photons were provided to the photodetector, resulting in a higher number of generated electron-hole pairs. Consequently, in both cases, the photocurrent increased proportionally to the incident light intensity, as shown in Fig. 2 (a). However, the constant temperature (CT) approach estimated a higher output current, nearly 12% more. In the varying temperature (VT) approach, these higher currents led to higher temperatures, as seen in Fig. 2 (b). In Fig. 2 (c), we plot the quantum efficiency calculated with both approaches, assuming the photodetector is covered with SiO_2 to match the refractive index of the fiber and minimize reflectance from the device. The CT approach estimated the quantum efficiency to be close to 0.65, whereas the measured value is reported as 0.55.[5] The VT approach estimate, $\sim$ 0.53, is much closer to this experimental result. Since mobilities decrease, one might expect quantum efficiency to drop with increasing temperature. However, the narrowing of the bandgap with increasing temperature allows more photons to excite electrons. Additionally, the presence of more thermally-excited charge carriers at higher temperatures provides more carriers available for generation by incident photons. As a result, we observe a slight increase in quantum efficiency, as seen in the blue curve in Fig. 2 (c), similar to the experimental results.[27] Next, we plotted the phase noise calculated in Fig. 2 (d). The

modulation frequency and depth are 9 GHz and 100%, respectively. Since phase noise generally decreases with increasing currents, in both approaches, we first observe a decay in phase noise, followed by convergence. The phase noise calculated with the VT model is $8-10$ dBc/Hz higher than the constant temperature approach. In Fig. 2 (e), the continuous and dashed lines represent the broadband RF output power calculated at the five mentioned incident power levels for modulation frequencies from 0 to 40 GHz using VT and CT approaches, respectively. In all cases, RF output power first increases with modulation frequency, then decreases. However, the frequency where RF output becomes the maximum is higher for VT results than for CT results. In Fig. 2 (f), we plot the bandwidths as a function of incident power. The CT approach estimates the bandwidth to be around 16.5 GHz at low modulation frequencies, which then decreases, whereas the VT approach estimates much higher bandwidths, initially at 23.9 GHz, then decreasing to lower values. The experimentally reported value is 24 GHz.[5] Again, we observe that the VT approach provides a more realistic outcome.

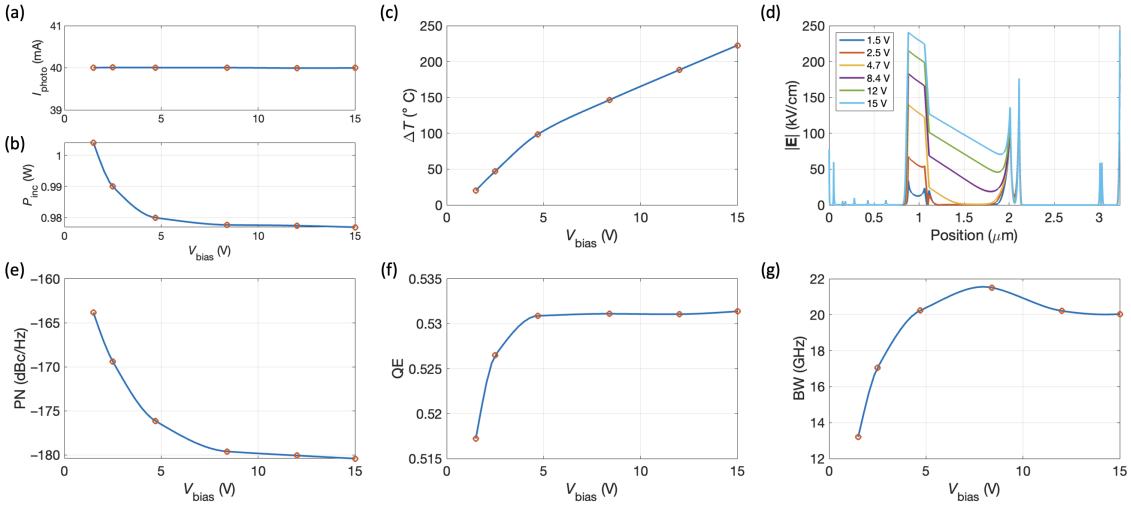

Figure 3. (a) MUTC2 photodetector produces the same photocurrent (I_{photo}) at different reverse biases (V_{b}) by adjusting the incident power (P_{inc}) to the values depicted in (b). (c) The temperature change (ΔT) at the n-contact, (d) electric field distributions, (e) phase noise, (f) quantum efficiency, and (g) bandwidth with increasing V_{b} as a function of reverse bias voltage.

Next, we examined the impact of the approximate temperature distribution on the photodetector's performance while producing the same photocurrent by varying the reverse bias. We followed our VT approach, assuming six different reverse bias values (1.5 V, 2.5 V, 4.7 V, 8.4 V, 12 V, and 15 V). For each bias value, a stable output photocurrent of 40 mA was achieved, as shown in Fig. 3 (a), by adjusting the incident power as depicted in Fig. 3 (b). Figures 3 (c) and (d) demonstrate that both the temperature and electric field intensity inside the absorber layers increase with rising bias voltage. These increasing electric fields accelerate the charge carriers, reducing their transit time through the photodetector. A reduced transit time spread leads to lower phase noise up to a certain point, as shown in Fig. 3 (e). The quantum efficiency of the photodetector, as depicted in Fig. 3 (f), slightly increases from 0.518 to 0.532 inversely to the decreasing incident power shown in Fig. 3 (b). At high power levels, where the incident power is near 1 W, the photodetector approaches saturation, and additional incident photons do not result in a proportional increase in generated electron-hole pairs. In Fig. 3 (g), we see that the bandwidth of the photodetector first increases and then decreases with bias voltage, similar to the previous studies.[9,27,28] This nonlinear dependence on bias voltage can be explained as follows: the temperature dependence of bandwidth is influenced by competing effects. As temperature rises, the bandgap narrows, allowing electrons to be excited with less energy, resulting in a wider bandwidth. However, the increased number of carriers generated by thermal energy at higher temperatures also leads to increased carrier recombination, which reduces the response time and bandwidth of the photodetector. The balance between these two competing effects determines the temperature dependence of the photodetector's bandwidth. If the goal is to achieve the widest bandwidth while producing an output current of 40 mA, then the modulation frequency of 7.8 GHz would be the ideal choice.

4. CONCLUSION

In summary, this study presents a numerical method to estimate temperature distribution in photodetectors under steady-state conditions. By using a simplified heat transport model, we examine how temperature changes affect key performance metrics like quantum efficiency, bandwidth, and phase noise. Our findings challenge the assumption of constant room temperature, showing that this can lead to overestimated current and efficiency, and underestimated bandwidth. Our model, which accounts for temperature variations, matches closely with experimental data. The low thermal conductivity of InGaAs is crucial in temperature buildup and performance changes. Additionally, varying reverse bias voltage reveals nonlinear effects on bandwidth, phase noise, and quantum efficiency. This validated numerical model enhances understanding of thermal management for high-power photodiodes, paving the way for further research in photodetector thermal characterization.

5. ACKNOWLEDGMENTS

This research was supported by Naval Research Laboratory under grant number N00173-21-1-G901.

REFERENCES

[1] Williams, K., Esman, R., and Dagenais, M., "Effects of high space-charge fields on the response of microwave photodetectors," *IEEE Photon. Tech. L.* **6**(5), 639–641 (1994).

[2] Ishibashi, T., Furuta, T., Fushimi, H., Kodama, S., Ito, H., Nagatsuma, T., Shimizu, N., and Miyamoto, Y., "InP/InGaAs uni-traveling-carrier photodiodes," *IEICE Trans. Electron.* **83**(6), 938–949 (2000).

[3] Jun, D.-H., Jang, J.-H., and Song, J.-I., "Effect of temperature on bandwidth and responsivity of uni-traveling-carrier and modified uni-traveling-carrier photodiodes," *Jpn. J. Appl. Phys.* **46**(4S), 2360 (2007).

[4] Li, Z., Fu, Y., Piels, M., Pan, H., Beling, A., Bowers, J. E., and Campbell, J. C., "High-power high-linearity flip-chip bonded modified uni-traveling carrier photodiode," *Opt. Express* **19**(26), B385–B390 (2011).

[5] Li, Z., Pan, H., Chen, H., Beling, A., and Campbell, J. C., "High-saturation-current modified uni-traveling-carrier photodiode with cliff layer," *IEEE J. Quantum Electron.* **46**(5), 626–632 (2010).

[6] Li, N., Li, X., Demiguel, S., Zheng, X., Campbell, J., Tulchinsky, D., Williams, K., Isshiki, T., Kinsey, G., and Sudharsansan, R., "High-saturation-current charge-compensated InGaAs-InP uni-traveling-carrier photodiode," *IEEE Photon. Tech. L.* **16**(3), 864–866 (2004).

[7] Beling, A., Xie, X., and Campbell, J. C., "High-power, high-linearity photodiodes," *Optica* **3**, 328–338 (Mar 2016).

[8] Moseley, C. et al., "Investigation of modified uni-traveling carrier photodiode for cryogenic microwave photonic links," *Opt. Continuum* **2**, 2215–2224 (Oct 2023).

[9] Zhou, G. and Runge, P., "Nonlinearities of high-speed p-i-n photodiodes and MUTC photodiodes," *IEEE Trans. Microw. Theory Tech.* **65**(6), 2063–2072 (2017).

[10] Kato, K., "Ultrawide-band/high-frequency photodetectors," *IEEE Trans. Microw. Theory Techn.* **47**(7), 1265–1281 (1999).

[11] Wang, X., Duan, N., Chen, H., and Campbell, J. C., "InGaAs–InP photodiodes with high responsivity and high saturation power," *IEEE Photon. Tech. L.* **19**(16), 1272–1274 (2007).

[12] Józwikowski, K., Musca, C., Faraone, L., and Józwikowska, A., "A detailed theoretical and experimental noise study in n-on-p $Hg_{0.68}Cd_{0.32}Te$ photodiodes," *Solid-State Electronics* **48**(1), 13–21 (2004).

[13] Jóźwikowski, K., Kopytko, M., Rogalski, A., and Jóźwikowska, A., "Enhanced numerical analysis of current-voltage characteristics of long wavelength infrared n-on-p hgcdte photodiodes," *J. Appl. Phys.* **108**(7) (2010).

[14] Fardi, H. Z., Winston, D. W., Hayes, R. E., and Hanna, M. C., "Numerical modeling of energy balance equations in quantum well Al_x /Ga_{1-x}/As/GaAs pin photodiodes," *IEEE Transactions on Electron Devices* **47**(5), 915–921 (2000).

[15] Li, G., André, N., Poncelet, O., Gérard, P., Ali, S. Z., Udrea, F., Francis, L. A., Zeng, Y., and Flandre, D., "Silicon-on-insulator photodiode on micro-hotplate platform with improved responsivity and high-temperature application," *IEEE Sensors Journal* **16**(9), 3017–3024 (2016).

[16] Rosbeck, J., Starr, R., Price, S., and Riley, K., "Background and temperature dependent current-voltage characteristics of HgCdTe photodiodes," *J. Appl. Phys.* **53**(9), 6430–6440 (1982).

[17] Dalapati, P., Manik, N. B., and Basu, A. N., "Effect of temperature on electro-optical characteristics of silicon based pn photodiode," *Silicon* **10**, 2547–2553 (2018).

[18] Brunk, M. and Jüngel, A., "Simulation of thermal effects in optoelectronic devices using coupled energy-transport and circuit models," *Math. Models Methods Appl. Sci.* **18**(12), 2125–2150 (2008).

[19] Wichman, A. R., DeWames, R. E., and Bellotti, E., "Three-dimensional numerical simulation of planar p+ n heterojunction $In_{0.53}Ga_{0.47}As$ photodiodes in dense arrays Part I: Dark current dependence on device geometry," in [*Infrared Technology and Applications XL*], **9070**, 10–30, SPIE (2014).

[20] Pisarenko, I. and Ryndin, E., "Numerical drift-diffusion simulation of GaAs pin and Schottky-barrier photodiodes for high-speed AIIIBV on-chip optical interconnections," *Electronics* **5**(3), 52 (2016).

[21] Malyshev, S. A., Chizh, A. L., and Vasileuski, Y. G., "High-power InGaAs/InP partially depleted absorber photodiodes for microwave generation," *J. Lightwave Technol.* **26**(15), 2732–2739 (2008).

[22] Simsek, E., Anjum, I. M., and Menyuk, C. R., "Solving drift diffusion equations on non-uniform spatial and temporal domains," in [*2023 Photonics & Electromagnetics Research Symposium (PIERS)*], 1644–1651 (2023).

[23] Simsek, E., Anjum, I. M., Carruthers, T. F., Menyuk, C. R., Campbell, J. C., Tulchinsky, D. A., and Williams, K. J., "Fast evaluation of RF power spectrum of photodetectors with windowing functions," *IEEE Trans. Electron. Dev.* **70**(7), 3643–3648 (2023).

[24] Simsek, E., Hastings, A. S., Tulchinsky, D. A., Williams, K. J., and Menyuk, C. R., "A simple numerical model to estimate the temperature distributions over photodetectors in steady-state," *IEEE Photonics Journal* **16**(3), 1–6 (2024).

[25] Kim, W., Zide, J., Gossard, A., Klenov, D., Stemmer, S., Shakouri, A., and Majumdar, A., "Thermal conductivity reduction and thermoelectric figure of merit increase by embedding nanoparticles in crystalline semiconductors," *Phys. Rev. Lett.* **96**, 045901 (Feb 2006).

[26] Anjum, I. M., Simsek, E., Mahabadi, S. E. J., Carruthers, T. F., Menyuk, C. R., Campbell, J. C., Tulchinsky, D. A., and Williams, K. J., "Use of evolutionary optimization algorithms for the design and analysis of low bias, low phase noise photodetectors," *J. Lightwave Technol.* **41**(23), 7285–7291 (2023).

[27] Chtioui, M., Lelarge, F., Enard, A., Pommereau, F., Carpentier, D., Marceaux, A., van Dijk, F., and Achouche, M., "High responsivity and high power UTC and MUTC GaInAs-InP photodiodes," *IEEE Photonic Tech. L.* **24**(4), 318–320 (2012).

[28] Chen, Y., Xie, Z., Huang, J., Deng, Z., and Chen, B., "High-speed uni-traveling carrier photodiode for 2 μm wavelength application," *Optica* **6**, 884–889 (Jul 2019).